Journal of Controlled Release 324 (2020) 633–643

Contents lists available at ScienceDirect

Journal of Controlled Release

journal homepage: www.elsevier.com/locate/jconrel

A peptide for transcellular cargo delivery: Structure-function relationship and mechanism of action

Alexander Komin[a,b], Maxim I. Bogorad[a,b], Ran Lin[a,c], Honggang Cui[a,c], Peter C. Searson[a,b,*], Kalina Hristova[a,b,*]

[a] Institute for Nanobiotechnology, Johns Hopkins University, 3400 North Charles Street, Baltimore, MD 21218, USA
[b] Department of Materials Science and Engineering, Johns Hopkins University, 3400 North Charles Street, Baltimore, MD 21218, USA
[c] Department of Chemical and Biomolecular Engineering, Johns Hopkins University, 3400 North Charles Street, Baltimore, MD 21218, USA.

ARTICLE INFO

Keywords:
Drug delivery
Transcellular transport
Cell-penetrating peptides
Polyarginine
Microvessel
Peptide proteolysis

ABSTRACT

The rate of transport of small molecule drugs across biological barriers, such as the blood-brain barrier, is often a limiting factor in achieving a therapeutic dose. One proposed strategy to enhance delivery across endothelial or epithelial monolayers is conjugation to cell-penetrating peptides (CPPs); however, very little is known about the design of CPPs for efficient transcellular transport. Here, we report on transcellular transport of a CPP, designated the CL peptide, that increases the delivery of small-molecule cargoes across model epithelium approximately 10-fold. The CL peptide contains a helix-like motif and a polyarginine tail. We investigated the effect of cargo, helix-like motif sequence, polyarginine tail length, and peptide stereochemistry on cargo delivery. We showed that there is an optimal helix-like motif sequence (RLLRLLR) and polyarginine tail length (R_7) for cargo delivery. Furthermore, we demonstrated that the peptide-cargo conjugate is cleaved by cells in the epithelium at the site of a two-amino acid linker. The cleavage releases the cargo with the N-terminal linker amino acid from the peptide prior to transport out of the epithelium. These studies provide new insight into the sequence requirements for developing novel CPPs for transcellular delivery of cargo.

1. Introduction

Systemic delivery of small molecule drugs usually involves crossing biological barriers, such as blood vessel walls and gastrointestinal walls, to reach the target site [1]. Thus, transport across the endothelium or epithelium is key to achieving a therapeutic dose. For example, transport across the blood-brain barrier (BBB) is a major roadblock in treating many central nervous system (CNS) diseases [2]. Drugs that are able to cross the BBB are generally limited to small, lipophilic molecules, making CNS drug development a formidable challenge [3].

One strategy to enhance delivery across the BBB and other biological barriers is to conjugate a candidate drug to a carrier, such as a cell-penetrating peptide (CPP) [4,5]. CPPs are short (typically < 40 amino acids) and frequently cationic [6,7]. Although they have been shown to enhance delivery of a variety of cargoes into cells [8], it is not clear whether fast cell uptake translates into fast transcellular transport where the delivery system must cross two cell membranes [9,10]. *In vivo* studies of transendothelial cargo delivery are often inconclusive, as they do not differentiate transport across the endothelium from sequestration in the endothelium. Previous *in vitro* studies using transwell assays have found low or no enhancement of cargo delivery using CPPs while maintaining barrier function [9,11].

Here, we investigated the role of peptide sequence on transcellular transport of cargoes (fluorescent probes) across epithelial monolayers. The peptides were based on a CPP sequence ($RLLRLLR_8$), that we designate the CL peptide, which has faster cell uptake than other CPPs, including Arg_9 and TP2. We systematically varied the sequence of the alpha helix region and the length of the polyarginine tail to elucidate the effect of arginine spacing, RLL repeats, hydrophobicity, hydrophobic moment, and charge. We show that the CL peptide has the optimal sequence for transcellular transport and that the mechanism involves proteolysis of the CL-cargo conjugates in the cell. Based on this work, we propose a mechanism for transcellular transport of peptide-cargo conjugates.

2. Materials and methods

2.1. Materials

Fmoc-Lys(Mtt)-OH, Fmoc-Arg(Pbf)-OH, and Fmoc-D-Arg(Pbf)-OH

* Corresponding authors at: Institute for Nanobiotechnology, Johns Hopkins University, 3400 North Charles Street, Baltimore, MD 21218, USA.
E-mail addresses: searson@jhu.edu (P.C. Searson), kh@jhu.edu (K. Hristova).

https://doi.org/10.1016/j.jconrel.2020.05.030
Received 15 April 2020; Accepted 20 May 2020
Available online 28 May 2020

were purchased from Chempep, Inc. (Wellington, FL). Rink-amide-MBHA, dichloromethane (DCM), and the remaining amino acids were purchased from Chem-Impex International, Inc. (Wood Dale, IL). PyAOP Novabiochem (Cat. no. 851221), HPLC-grade trifluoroacetic acid (TFA), hexafluoroisopropanol (HFIP), synthesis-grade phenol, and N,N-Diisopropylethylamine (DIPEA) were purchased from Millipore Sigma (Burlington, MA). Triisopropylsilane (TIS) was purchased from Oakwood Products, Inc. (Estill, SC). 5-Carboxyfluorescein (5FAM; Cat. no. AS-81003) was purchased from Anaspec, Inc. (Fremont, CA). 5-(and-6)-Carboxytetramethylrhodamine, mixed isomers (5(6)TAMRA; Cat. no. C300), Lucifer yellow CH-lithium salt (Cat. no. L-453), Corning UltraLow Attachment plates (Cat no. 3473), Eppendorf Protein LoBind tubes (Cat. no. E925000090) were purchased from Thermo Fisher Scientific (Waltham, MA). IR800CW NHS ester (Cat. no. 929-70020) was purchased from LI-COR Biosciences (Lincoln, NE). POPC (Cat. no. 850457) and POPG (Cat. no. 840457) were purchased from Avanti Polar Lipids, Inc. (Alabaster, AL).

2.2. Peptide synthesis

The peptides were synthesized using Fmoc solid-phase synthesis techniques, conjugated to cargo, and purified, as described in Supplemental methods 1 (see Fig. S1 for chemical structures). Arg_9-5FAM (Cat. no. AS-61207) was purchased from Anaspec, Inc. (Fremont, CA). TP2-6TAMRA maleimide was provided by Dr. William Wimley (Tulane University). All peptides were treated with 0.1% HCl for 10 min to remove TFA. Peptide purity was characterized by RP-HPLC and peptide molecular weights were measured by MALDI-TOF (see Supplemental methods 1, Fig. S2). The lyophilized peptides were re-suspended in HFIP/water (5:1) (v/v) and their stock concentrations were measured by absorbance in solvents with the reported extinction coefficients (methanol for 6TAMRA and IR800CW conjugates; 50 mM potassium phosphate buffer, pH 9, for 5FAM conjugates). The peptides were aliquoted in HFIP/water (5:1) (v/v) into Protein LoBind tubes, dried under nitrogen flow, and further dried overnight in a vacuum chamber, followed by storage in a −20 °C freezer.

2.3. Cell culture

MDCKII cells were obtained from the Netherlands Cancer Institute and were used in experiments from P19 to P40. The cells were cultured in DMEM (high glucose, GlutaMax supplement) (Cat. no. 10566016, Thermo Fisher Scientific), supplemented with 10% FBS (Cat. no. F4135, Sigma-Aldrich) and 1% PenStrep (Cat. no. 15140122, Thermo Fisher Scientific).

2.4. Confocal microscopy

Nunc Lab-Tek II glass 8-chamber slides (Cat. no. 155409, Thermo Fisher Scientific) were coated with 30 μg cm^{-2} rat-tail collagen I (Cat no. 354249, Corning) in 0.02 M acetic acid at 4 °C overnight. MDCKII cells were seeded at 5.7×10^4 cells cm^{-2} and were cultured for 2–3 days with a daily DMEM (10% FBS, 1% PenStrep) change. On day 2–3, the cells were incubated in medium containing 2 μg mL^{-1} Hoechst 33342 nuclear stain (Cat. no. 62249, Thermo Fisher Scientific) for 30 min at 37 °C, 5% CO_2. Afterwards, the cells were washed with 1× Hank's Balanced Salt Solution (HBSS) buffer (1× HBSS, 15 mM D-glucose, 10 mM HEPES, pH 7.4) three times and the peptides were added at 2.5 μM concentration in HBSS buffer. 1xHBSS contains 3.5 g L^{-1} sodium bicarbonate. The cells were incubated with the peptides for 1 h at 37 °C, 5% CO_2, after which the cells were washed three times with HBSS buffer. To assess peptide accumulation inside cells, sub-confluent monolayers of MDCKII cells were imaged while incubated with peptide or dye in HBSS buffer at 37 °C. The cell borders were traced based on phase contrast images and Hoechst 33342 staining. Confocal images of live cells were obtained on an inverted Nikon TiE microscope equipped with a swept field confocal microscope system (Prairie Technologies) and MLC 400 monolithic laser combiner (Keysight Technologies). The imaging was performed in a 37 °C chamber using a 60× oil objective and NIS Advanced Research software (Nikon, Tokyo, Japan). The fluorophores were excited at 405 nm and 561 nm.

2.5. Immunocytochemistry

Cells were cultured on collagen-coated glass chamber slides and on day 3 were treated with CL-cargo conjugate and HBSS buffer as described in section 2.4. After the treatment, the cells were washed with 1xPBS azide and fixed in 3.7% paraformaldehyde solution for 10 min. The fixed cells were washed with 1xPBS azide and incubated in blocking solution (10% goat serum, 0.3% TritonX-100 in 1xPBS azide) at 4 °C overnight. The cells were incubated with anti-ZO1 primary antibody (Cat. no. 40-2200, Thermo Fisher Scientific) at 1:200 dilution for 2 h at room temperature. Afterwards, the cells were washed three times, 5 min each, with PBS azide, and incubated with the secondary Alexa Fluor 488-labeled antibody (Cat. no. A11008, Thermo Fisher Scientific) at 1:200 dilution for one hour at room temperature, followed by three 5-min washes. After the incubation, the cells were stained with Fluoromount G, containing DAPI (Cat. no. 00-4959-52, Thermo Fisher Scientific). Epifluorescence images were acquired with an inverted microscope Nikon TiE using 10× objective and NIS Advanced Research software (Nikon, Minato, Tokyo, Japan).

2.6. Permeability measurements in transwells

2.6.1. Sample preparation

Dried peptide aliquots were resuspended in HBSS buffer shortly before the experiment and sonicated briefly. One hydrophobic peptide conjugate, TP2-6TAMRA maleimide, was first resuspended in DMSO and further diluted with HBSS buffer resulting in 1% DMSO final concentration. IR800CW NHS ester dye was neutralized overnight in 1xPBS prior to the permeability experiment.

2.6.2. Transwell assay

MDCKII cells were seeded on rat-tail collagen I-coated PET transwells (Cat. no. 3470, Corning) in DMEM (10% FBS, 1% PenStrep), as described previously [12], and were allowed to adhere for 1 h followed by a wash with the medium. The cell medium was then changed daily. Permeability measurements were performed on day 3 after seeding. Cells were washed with and incubated in DMEM (10% FBS, 1% PenStrep) for 2 h, followed by a wash and 30-min incubation in 1× Hank's Balanced Salt solution (HBSS) buffer (1xHBSS, 15 mM D-glucose, 10 mM HEPES, pH 7.4). The peptide-cargo conjugates and the free cargo were added to the apical chamber with HBSS buffer in the basolateral side, and placed on a rocker in an incubator at 37 °C, 5% CO_2 for 1 h. The transwell assays were performed in ultra-low attachment (ULA) 24-well plates, pre-coated with DMEM (10% FBS, 1% PenStrep) for at least 2 days to decrease peptide sequestration.

2.6.3. Permeability measurements

The concentrations of the peptide-cargo conjugates and the unconjugated cargo (5FAM, 5(6)TAMRA, IR800CW) were measured by fluorescence in medium-precoated ULA plates. We also determined the permeability of Lucifer yellow (LY), which is widely used to assess barrier integrity. The fluorescence of the solution in the basolateral chamber was measured after 1 h. We verified that for all solutes the concentration was less than 10% of the input concentration, i.e. the concentration was in the linear regime [13]. For 5FAM and 6TAMRA conjugates and the unconjugated cargo, fluorescence was measured using a Synergy H4 plate reader (Biotek Instruments Inc., Winooski, VT). For IR800CW conjugates and IR800CW cargo, fluorescence was measured using an Odyssey CLx infrared imaging system (LI-COR Biosciences) and Image Studio Lite Software 5.2.5. The apparent

permeability (P_{app}) was calculated from:

$$P_{app} = \frac{dQ}{dt}\frac{V}{A}\frac{1}{C_o} \quad (1)$$

where dQ/dt is the increase in fluorescence in the basolateral chamber, V is the volume of the basolateral chamber, A is the surface area of the transwell filter, and C_o is the initial concentration of the cargo in the apical chamber.

2.6.4. Transepithelial electrical resistance measurements

Monolayer integrity was assessed by measuring transepithelial electrical resistance (TEER) before and after the permeability experiments. TEER was measured for monolayers in HBSS buffer using an Evom-2 and Endohm-6 chamber (World Precision Instruments, Sarasota, FL). TEER was reported after subtracting the resistance of a blank collagen-coated transwell from the measured TEER and multiplying the result by the transwell area. TEER values after the permeability experiment were 45–75 Ω cm^2 for all peptide-cargo conjugates, with the exception of four peptides that had TEER below 45 Ω cm^2 (Fig. S3).

2.6.5. Mass balance

Following the permeability measurements, solution samples from the apical chamber were collected and diluted in HBSS buffer directly in medium-precoated ULA plates for fluorescence measurements to assess mass balance. We determined 40–80% recovery for the majority of the peptide-cargo conjugates and 70–80% recovery for the unconjugated cargo (Fig. S4).

2.7. Permeability measurements in tissue-engineered microvessels

Permeability measurements were also performed in tissue-engineered microvessels, fabricated using protocols that we have reported previously [14]. For live cell imaging and time-lapse microscopy, the platform was mounted in a custom-built microscope stage in a live cell chamber on an inverted microscope (Nikon TiE) and maintained at 37 °C and 5% CO_2. Phase contrast and fluorescence images were recorded for about 5 min to establish background conditions. Lucifer yellow (LY) was injected into the flow loop at a concentration of 100 μM, and phase contrast and fluorescence images were recorded for 45–90 min to capture the initial increase in intensity when the solute reached the microvessel and the following distribution of the solute in the cells and surrounding matrix. The time for the solute to reach the microvessel from the medium reservoir was about 30 s. Following the imaging, LY was washed out from the vessel, the background was imaged, and CL-6TAMRA, TP2-6TAMRA, or DCL-6TAMRA were injected into the medium reservoir at a concentration of 2.5 μM. All images were recorded at 2 min intervals, selected to achieve maximum resolution for analysis of the transport kinetics and to avoid photobleaching. All fluorescence images were obtained using filter set ET-Sedat Quad-band (8900, Chroma Technology Crop). LY was imaged using a 20× objective and excitation/emission filters ET402/ET525 at 60 ms exposure. CL-6TAMRA and DCL-6TAMRA were imaged using a 20× objective and excitation/emission filters ET555/ET605 at 350 ms exposure and 4× gain.

2.8. Peptide physico-chemical property calculations

Peptide hydrophobicity and hydrophobic moment were calculated using the Wimley-White scale for peptide partitioning from water into the lipid bilayer interface (MPEX v. 3.2.15) [15]. The results are summarized in Table S1, along with molecular weight and charge.

2.9. Peptide digestion study

To determine whether the peptide-cargo conjugates remained intact following transcellular transport, we used HPLC to analyze the contents of the basolateral chamber following permeability experiments. In these experiments, the permeability was measured in Corning PTFE collagen-coated transwells (Cat. no. 3495), which allowed us to collect twice as much basolateral product than when we used PET collagen-coated transwells. The peptide-cargo conjugates were added to the apical side at 2.5 μM concentration and the permeability experiment was run for 1 h. The basolateral solution was collected into Protein LoBind Eppendorf tubes, frozen in liquid nitrogen, and stored in a −20 °C freezer. The major fluorescent fraction, monitored by a fluorescence detector (ex/em 542/566 nm for 6TAMRA and 492/519 nm for 5FAM) was purified on an Agilent 1260 Infinity Quaternary HPLC system [binary gradient: water with 0.1% TFA (solvent A), acetonitrile with 0.1% TFA (solvent B); flow rate: 1 mL/min; 0–28 min gradient 5% to 60% B; 28–29 min gradient 60% to 5% B; 29–30 min isocratic 95% A, 5% B; Agilent Zorbax 300SB C18 analytical column, 5 μm, 4.6 mm × 250 mm]. The collected fraction was lyophilized and resuspended in LC-MS grade water. The mass spectrometry of the fraction was performed on Waters Acquity H-class UPLC system in tandem with a Xevo-G2 high mass resolution Q-TOF–MS/MS–ESI system. ES+ [ternary gradient: water (solvent A), acetonitrile (solvent B), 1% formic acid in water (solvent C); flow rate: 0.3 mL/min; 0–1 min isocratic 90% A, 10% C; 1–7.5 min gradient 0% to 80% B, isocratic 10% C; 8.4–8.5 min gradient 80% to 0% B, isocratic 10% C; 8.5–10 min isocratic 90% A, 10% C. Waters Acquity UPLC BEH C18 Column, 1.7 μm, 2.1 mm × 50 mm]. During the first minute, the flow from the column was diverted away from the mass spectrometer into the waste to further remove salts from the sample. Mass analysis was carried out using MassLynx software.

2.10. Circular dichroism

Peptide circular dichroism spectra were collected using Jasco J-710 spectropolarimeter (Easton, MD). The peptides were resuspended in 10 mM sodium phosphate buffer, pH 7, at 10 μM concentration. Peptide spectra were measured from 280 nm to 180 nm at the scanning speed of 100 nm/min, data pitch 0.1 nm, response 4 s, and bandwidth 1 nm. The spectra were measured 5 times and averaged. To measure circular dichroism spectra of peptides in the presence of lipid vesicles, we prepared 100 nm POPC and 10%POPG/90%POPC vesicles. Briefly, the synthetic lipids in chloroform were dried into a thin film under a nitrogen flow in a glass vial, followed by overnight drying in a vacuum chamber. The lipids were later resuspended in 10 mM sodium phosphate buffer, pH 7, and extruded ten times through a polycarbonate filter to form 100 nm vesicles. The lipid concentrations in the vesicles were quantified using a modified Stewart assay [16]. The vesicles were incubated with the peptide solution in buffer prior to measurement of circular dichroism spectra.

2.11. Oriented circular dichroism

The CL peptide, resuspended in spectrophotometric-grade methanol, and POPC lipids, resuspended in chloroform, were mixed at 1:50 (peptide:lipid) ratio. The mixture was deposited on quartz disk one droplet at a time, allowing for the mixture to dry between the additions. The slide was assembled into a custom chamber and was dried in the lyophilizer for 1 h to remove the solvents. The mixture was hydrated with vapor from a water drop in the chamber for 30 min, and 8 spectra were collected with 45° axial rotations of the chamber between the scans. The spectra were measured from 260 nm to 180 nm at the scanning speed of 50 nm/min, data pitch 0.5 nm, response 2 s, and bandwidth 2 nm.

2.12. Statistical analysis

One-way ANOVA with post-hoc Tukey HSD test and the partial

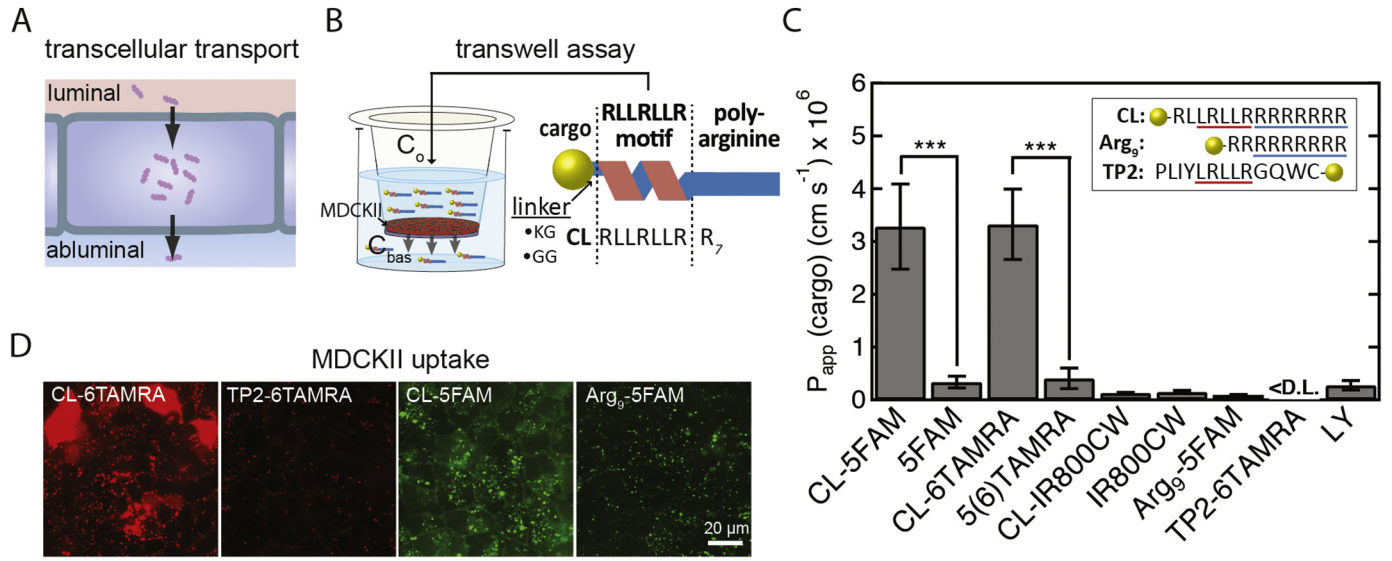

Fig. 1. Transcellular transport of cargo across cell monolayers using cell-penetrating peptides. A. Schematic illustration of transport across an endothelial or epithelial monolayer where tight junctions restrict paracellular transport. B. Schematic illustration of the CL peptide and the transwell assay. The CL peptide contains an RLLRLLR motif and a polyarginine tail (R_7). Fluorescent probes (cargoes) are conjugated to the peptide N-terminus via a Lys(acetyl)-Gly or a Gly-Gly linker. The permeability (P_{app}) of the cargo is measured in the transwell assay, in which a monolayer of MDCKII cells is grown on a porous filter. P_{app} is calculated from the initial apical concentration (C_o) and the concentration in the basolateral chamber after 1-h incubation (see text for details). C. The permeability of fluorescent probes and peptide-cargo conjugates across MDCKII cells. The CL peptide significantly enhanced P_{app} for 5FAM and 6TAMRA but not for IR800CW. Insert: Sequences of the CL peptide, Arg_9 (a commonly-studied cell-penetrating peptide), and TP2, with which the CL peptide has sequence homology. The integrity of the MDCKII monolayer was confirmed by measurements of the permeability of Lucifer yellow (LY) and unconjugated cargoes. The apical concentrations were 2.5 µM for peptide-cargo conjugates, 10 µM for 5FAM, 20 µM for 5(6)TAMRA, and 100 µM for LY. < D.L. = below the detection limit. Data represent mean ± SD. The sample size n represents the number of transwell replicates: CL-5FAM (n = 27), 5FAM (n = 20), CL-6TAMRA (n = 40), 5(6)TAMRA (n = 39), CL-IR800CW (n = 4), IR800CW (n = 4), Arg_9-5FAM (n = 3), TP2-6TAMRA maleimide (n = 4), LY (n = 7). ***p < .001 (Student's *t*-test, two-tailed, unequal variance). D. Fluorescence confocal microscopy images of the uptake of CL-6TAMRA, TP2-6TAMRA-, CL-5FAM, and Arg_9-5FAM in MDCKII cells after 1-h incubation at 37 °C (see Fig. S7 for nuclear stain and additional images). The concentration of CL-cargo conjugates in the MDCKII cells is greater than the concentration of TP2 and Arg_9 conjugates. CL conjugates exhibit a diffuse and punctate fluorescence inside cells whereas TP2 and Arg_9 conjugates exhibit mostly punctate fluorescence. (For interpretation of the references to colour in this figure legend, the reader is referred to the web version of this article.)

correlation analysis ("ppcor" package v 1.1) was performed in the R statistical computing package using RStudio (v 3.5.1–3.5.2). Student's *t*-tests were performed using Microsoft Excel.

3. Results

3.1. Cargo permeability in a transwell assay

The CL peptide was designed to effectively deliver cargo into cells [17]. The peptide contains a helix-like motif and a polyarginine tail (R_7). Arginines and leucines were selected for their propensities to form alpha helices. Experimental data suggest that they have approximately equal ability to promote helix formation [18]. To determine whether the peptide could also enhance transcellular transport across an epithelial monolayer (Fig. 1A), we measured the permeability of CL peptide-cargo conjugates in a transwell assay with a monolayer of MDCKII cells (derived from canine kidney epithelial cells) (Fig. 1B). Transcellular permeability across MDCKII monolayers is widely used to assess drug penetration into the brain [19,20].

We confirmed by daily TEER measurements that MDCKII cells form a stable, confluent monolayer by day 3 after seeding on a transwell (Fig. S5). On day 3, we determined the permeability of the CL peptide conjugated to three fluorescent cargoes: 5FAM, 6TAMRA, and IR800CW (Fig. 1C). The peptide was conjugated to the cargo via a Gly-Gly linker or a Lys(acetyl)-Gly linker, and the choice of linker was shown to have no effect on the permeability (Fig. S6). The unconjugated cargoes had low permeability (P_{app}), similar to Lucifer yellow, which is commonly used to validate the barrier integrity [12,21]. In contrast, we measured 10-fold higher values for CL-5FAM conjugates and 8-fold higher values for CL-6TAMRA conjugates. While similar in size, 6TAMRA (MW = 430.5 Da) is moderately hydrophobic and 5FAM (MW = 375.3 Da) is moderately hydrophilic, demonstrating that the CL peptide can deliver both types of molecules [22]. Interestingly, the CL peptide did not significantly enhance P_{app} of the larger IR800CW cargo (MW = 1097.2 Da), an infrared dye commonly used for *in vivo* imaging. These results suggest that the CL peptide can enhance the delivery of small-molecule cargo; however, there are some limits on what cargo can be delivered.

The CL peptide shares sequence similarities with the Arg_9 and TP2 peptides (Fig. 1C). These three peptides are rich in leucines and arginines. Typically, leucines are used to increase hydrophobicity and help mediate the interactions with the hydrophobic core of the membrane [23]. Arginines are used to incorporate positive charges, and are thought to interact with negatively charged sugar groups on the membrane surface and with the phosphate groups of the lipids [24]. In the literature, Arg_9 has been demonstrated to deliver a variety of cargo into cells by endocytosis [25–28]. The CL and TP2 peptides share an LRLLR sequence motif, which is thought to be the minimum sequence for direct translocation across lipid membranes without permeabilization [26,29,60]. Thus, the sequence of the CL peptide combines characteristics of both Arg_9 and TP2.

The CL peptide had a significantly larger permeability than the Arg_9 and TP2 peptides (Fig. 1C), which suggests that the polyarginine tail and the LRLLR motif cannot individually explain the increase. Thus, it appears that the CL peptide has a unique sequence that enables transcellular cargo delivery. We also observed lower cell uptake for Arg_9- and TP2-cargo conjugates when compared to the CL-cargo conjugates (Fig. 1D, Fig. S7). It is possible that the low P_{app} of cargo conjugated to Arg_9 and TP2 is due to low cell uptake.

Transepithelial electrical resistance (TEER) is widely used to

measure junctional integrity in confluent monolayers, where a decrease in TEER is indicative of the formation of defects or a global decrease in junctional integrity [30]. We measured TEER before and after the treatment with peptide-cargo conjugates to assess their effect on junctional integrity (Fig. S3). Treatment with CL-cargo conjugates during the permeability experiment did not result in decrease in junctional integrity. We also assessed the effect of CL-cargo conjugate treatment on the expression of a tight junction protein, Zona occludens-1 (ZO-1), and confirmed that expression was similar to the untreated control (Fig. S8). In addition, we assessed the long-term effect of the CL-cargo conjugate on junctional integrity by measuring the permeability of LY and TEER 4 h and 24 h after treatment (Fig. S9). We measured a low LY P_{app} of 2–3 $\times$ 10^{-7} cm s^{-1} at both time points, consistent with the measurements for an intact barrier. TEER measurements after the treatment were similar to the initial values, further confirming maintenance of barrier integrity. These results demonstrate that the CL peptide does not have a long-term effect on junctional integrity and suggests that the CL-cargo conjugate has low cytotoxicity.

3.2. Permeability measurements in tissue-engineered microvessels

In a transwell assay, permeability is measured under static conditions. Furthermore, the porous plastic filter in the transwell assay can sequester solutes and hence affect permeability values [31,32]. Therefore, we sought to confirm our findings under more physiological conditions. To do so, we studied the permeability of CL-6TAMRA and TP2-6TAMRA in a tissue-engineered microvessel model. In this model, MDCKII cells are seeded into a cylindrical channel in an extracellular matrix (ECM) to form a perfusable lumen (Fig. 2 A–C) [14,]. The tissue-engineered microvessel model recapitulates the cylindrical geometry, continuous flow in the lumen, and a 3D extracellular matrix. Microvessels were perfused at a flow rate of 0.2 mL h^{-1}, corresponding to a wall shear stress of 1.7 dyne cm^{-2}, typical of post-capillary venules. In these experiments the peptide-cargo conjugate was introduced into the flow loop and the permeability was determined from the fluorescence intensity in the surrounding matrix at the lumen midplane using previously published protocols (Fig. 2 D–E) [14,34]. In each experiment, the microvessel was first perfused with Lucifer yellow (LY) to verify barrier integrity. In all cases, the LY permeability was 2.6 $\pm$ 0.9 $\times$ 10^{-7} cm s^{-1}, consistent with previously reported values (Fig. 2 E–F) [14]. We measured P_{app} = 3.2 $\pm$ 0.8 $\times$ 10^{-6} cm s^{-1} for CL-6TAMRA (Fig. 2 E–F) and P_{app} = 4.6 $\times$ 10^{-7} cm s^{-1} for TP2-6TAMRA (data not shown). Thus, CL-6TAMRA has 7-fold greater permeability than TP2-6TAMRA. There was no statistically significant difference between the measurements in the microvessel and the transwell models for both LY and CL-6TAMRA (Fig. 2F). These results show that the transwell measurements are very similar to measurements under physiological conditions and that sequestration of the conjugates was not significant.

3.3. Structure-function studies

Having established that the CL peptide can increase transcellular transport of 5FAM and 6TAMRA, we next investigated how the sequence and structure of the peptide influence transcellular cargo delivery. It has been suggested that the RLLRLLR motif and a polyarginine tail in the CL peptide form an alpha helix and a polyproline-II-like secondary structure, respectively [17]. To further probe the secondary structure, we measured the oriented circular dichroism (OCD) spectrum of the CL peptide in stacked lipid bilayers, which provided additional information on whether the peptide is inserted perpendicular to the lipid bilayer or is aligned parallel to the bilayer surface [35]. For OCD measurements, the CL peptide was co-dissolved with POPC lipids in organic solvents and the mixture was dried on the glass slide, resulting in the formation of stacked lipid bilayers with the peptide intercalated within the lipid sample. The OCD spectrum of the hydrated sample had two minima at 208 nm and 222 nm, which indicates that the CL peptide can form an alpha helix and that it is oriented parallel to the lipid bilayer (Fig. S10A). We next measured circular dichroism (CD) spectra of the CL peptide in buffer and in the presence of 100 nm lipid vesicles.

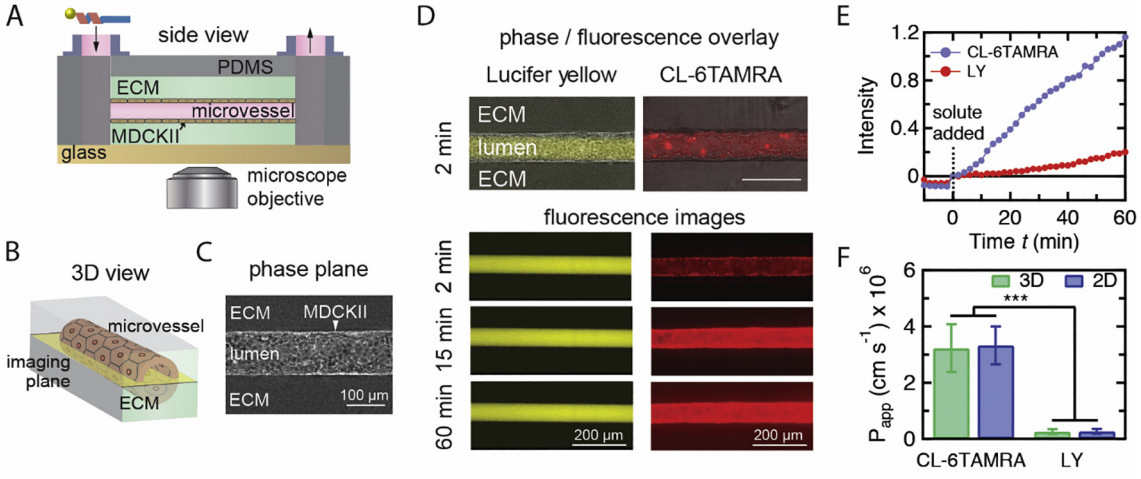

Fig. 2. Measurements of permeability of CL-6TAMRA in a tissue-engineered microvessel model. A. Schematic illustration of an MDCKII microvessel embedded in a collagen gel within a PDMS housing. The peptide-cargo conjugate was introduced in the inlet and perfused through the microvessel lumen by gravity flow during real-time imaging on an epifluorescence microscope. B. Schematic illustration showing the microvessel midplane used for imaging. C. Phase contrast image of an MDCKII microvessel. D. Phase-fluorescence overlays and fluorescence images of the microvessel at different times following injection of 2.5 µM CL-6TAMRA or 100 µM Lucifer yellow. E. Normalized fluorescence intensity in the extracellular matrix (ECM) versus time for representative perfusions of Lucifer yellow (LY) and CL-6TAMRA. The fluorescence is normalized to the lumen intensity at t = 2 min. CL-6TAMRA or LY were added at time t = 0 min and the microvessel was imaged for 1 h. Images prior to the injection (t < 0 min) were used to measure the background fluorescence. The permeability of CL-6TAMRA and LY was calculated from the slope of the linear fit to the intensity measurements after background subtraction. F. The permeability of CL-6TAMRA and LY measured in the microvessel platform (3D) and the transwell assay (2D). The permeability of CL-6TAMRA was about 3 $\times$ 10^{-6} cm s^{-1} in both 3D and 2D. The LY permeability of about 3 $\times$ 10^{-7} cm s^{-1} confirms barrier integrity. The sample size n represents the number of microvessels or transwell replicates: CL 3D (n = 3), CL 2D (n = 40), LY 3D (n = 6), LY 2D (n = 7). Data represent mean $\pm$ SD. ***p < .001 (One-way ANOVA with post-hoc Tukey HSD test). (For interpretation of the references to colour in this figure legend, the reader is referred to the web version of this article.)

The CD spectra of the CL peptide in the presence of neutral POPC vesicles and in the absence of vesicles has a minimum close to, but not exactly at, 200 nm. This indicates that the CL peptide exists largely as a random coil, but with an additional secondary structure contribution (Fig. S10B). POPG lipids are negatively charged and have been shown to promote the binding and secondary structure formation of cationic peptides [36,37]. The CD spectrum of the CL peptide in the presence of 10%POPG/90%POPC vesicles showed a strong alpha helical contribution (Fig. S10B).

To further understand the contribution of the RLLRLLR motif to the secondary structure, we compared the CD spectrum of the CL peptide to Arg_9. The CD spectrum of Arg_9 in buffer shows that it is largely a random coil with a minimum at 200 nm, while the CL peptide has an additional secondary structure contribution (Fig. S10C). Taken together with the OCD spectrum and the solution CD spectrum in the presence of POPG-containing vesicles, as well as the previously measured helical spectra in membrane-mimetic solution [17], we conclude that the RLLRLLR motif is alpha helical. We will further refer to this motif as a helix-like motif.

To gain insight into the significance of alpha helix formation for transcellular cargo delivery, we designed a peptide with the sequence $RLLrLLR_8$, designated CLr, in which the second arginine in the RLLRLLR motif is replaced with a D-isomer of arginine. The CLr peptide has the same primary sequence as the CL peptide but cannot form an alpha helix, as confirmed from the CD spectra (Fig. 3A). The permeabilities for CLr-5FAM and CLr-6TAMRA were significantly lower compared to the corresponding conjugates with the CL peptide (Fig. 3B).

These results suggest that alpha helix formation is important in enhancing transcellular cargo transport. Furthermore, these results suggest that the alpha helical structure potentiates the insertion of the RLLRLLR motif into the membrane. It is well known that the peptide backbone, when not participating in hydrogen bonds, is polar and costly to insert in the membrane [38]. Hydrogen bonding upon secondary structure formation significantly reduces the thermodynamic penalty of backbone partitioning into the membrane.

3.4. Helix-like motif sequence

To explore the effect of the helix-like motif sequence on permeability in the transwell assay, we synthesized a panel of peptides. For the purpose of these experiments, we assumed that the RLLRLLR motif forms an alpha helix and that the polyarginine tail (R_7) forms a random coil. In the alpha helix conformation, the arginines and leucines in the motif are positioned on different faces of the alpha helix making it amphipathic. Amphipathic alpha helices are known to partition into the interface of lipid bilayers and are frequently present in CPPs [6,7,38]. We hypothesized that transcellular transport was related to the physico-chemical properties of the helix-like motif. To test the hypothesis, we synthesized peptides in which we varied the arginine content, arginine spacing, the number of RLL repeats, and leucine substitutions in the helix-like motif. These modifications resulted in differences in the calculated physico-chemical properties, such as hydrophobicity, hydrophobic moment, and charge (Table S1).

First, we sought to measure the contribution of the second arginine in the helix-like motif to transcellular cargo delivery by replacing it with a leucine ($RLLLLLR_8$). Leucine has the same propensity for alpha helix formation as arginine, but it lacks the charged guanidinium group [18]. The substitution resulted in similar secondary structure as the CL peptide, but significantly decreased P_{app} (Fig. 4A, Fig. S11). The presence of arginine is likely important because it provides an additional charge and greatly contributes to the high hydrophobic moment of the alpha helix.

Next, we explored the effect of arginine spacing in the helix-like motif on P_{app}. It was previously demonstrated that increasing the arginine density in the alpha helix can increase intracellular cargo delivery [39]. The spacing between the arginines in the helix-like motif changes the arginine density of the alpha helix. Furthermore, higher arginine density is reflected in higher calculated hydrophobic moment. For example, we synthesized the peptide RLLRLLLR with higher hydrophobic moment when compared to the original motif because it has three arginines distributed among two faces of the alpha helix; however, this modification did not increase P_{app}. A further increase in the arginine spacing (RLLLRLLLR) resulted in a hydrophobic moment similar to that of the CL peptide but a decrease in P_{app} (Fig. 4A). The $RLLLRLLLR_8$ peptide has a longer and more hydrophobic alpha helix that could affect transcellular cargo delivery. Decreasing the spacing between the arginines (LRLRLR) resulted in a random coil-like secondary structure and the lowest P_{app} (Fig. S11). This result is consistent with our finding that the secondary structure formation is important for high P_{app} (Fig. 3).

The sequence modifications of the RLLRLLR motif can result in changes in multiple physico-chemical parameters (e.g. hydrophobicity, hydrophobic moment, charge, % helicity). Both alpha helix hydrophobicity and hydrophobic moment are thought to affect the peptide binding to cell membranes and intracellular components [7,37,38,40], and hence we next explored the effect of these parameters on transcellular transport. In particular, it has been proposed in the literature that the efficiency for membrane translocation depends on the hydrophobicity of the peptide. As a consequence, a very hydrophobic peptide will likely partition into the membrane and remain associated with the membrane, rather than translocate [37]. We therefore tested if changes in peptide hydrophobicity affect translocation efficiency.

We synthesized a panel of peptides where a single leucine in the helix-like motif was replaced with either valine, tyrosine, or tryptophan (Fig. 4B). We chose the position of the leucine replacement that resulted in the highest calculated hydrophobic moment ($RLLRLWR_8$, $RLLRLYR_8$,

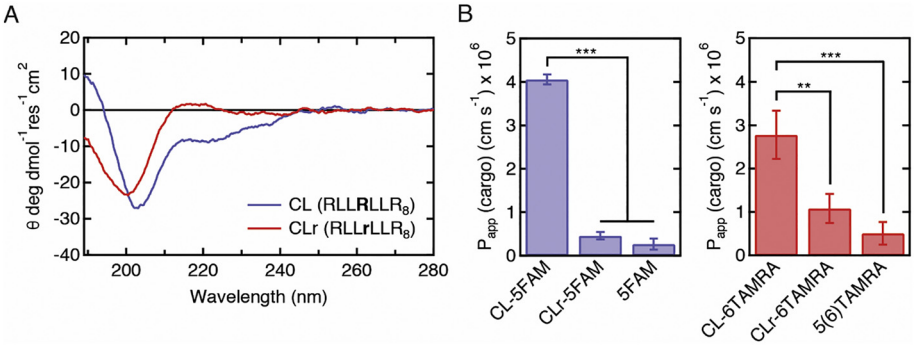

Fig. 3. The role of helix-like secondary structure in transcellular transport of peptide-cargo conjugates across MDCKII monolayers. A. Circular dichroism spectra of the CL peptide and a variant with a single D-arginine substitution in the helix-like motif (CLr). The spectra were measured for 10 μM peptide-cargo conjugate solutions in 10 mM sodium phosphate buffer, pH 7. The D-arginine substitution in CLr eliminated the secondary structure. B. The permeability of peptide-cargo conjugates (CL-5FAM, CL-6TAMRA, CLr-5FAM, and CLr-6TAMRA) and free cargo (5FAM and 5(6)TAMRA). The D-arginine substitution significantly decreased the permeability of CLr-cargo conjugates, suggesting that alpha helix formation may be important for the efficient cargo delivery by the CL peptide. The apical concentrations were 2.5 μM for the peptide-cargo conjugates, 10 μM for 5FAM, and 20 μM for 5(6)TAMRA. Sample size n represents the number of transwell replicates: n = 3 for all treatments. Data represent mean ± SD. **p < .01, ***p < .001 (one-way ANOVA with post-hoc Tukey HSD test).

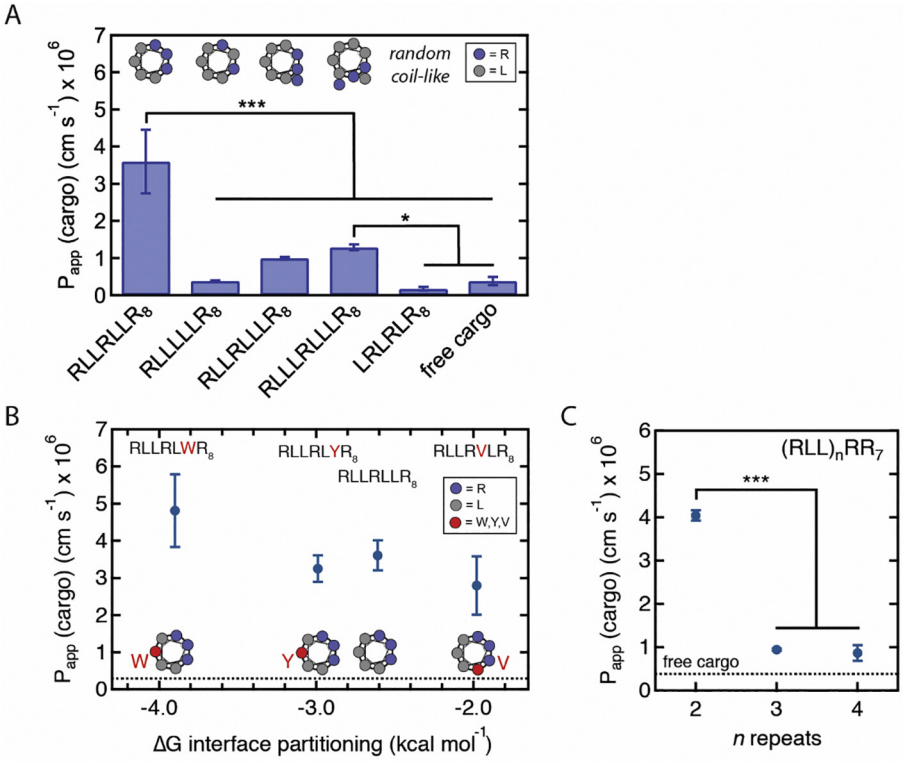

Fig. 4. The effect of the helix-like motif sequence on the permeability of peptide-cargo conjugates across MDCKII monolayers in a transwell assay. A. The permeability of peptide-5FAM conjugates with different arginine spacing in the alpha helix. The apical concentrations were 2.5 μM for the peptide-cargo conjugates and 10 μM for 5FAM. Helical wheel diagrams, assuming full helicity, show leucines in gray and arginines in purple. The arginine-to-leucine substitution significantly decreased P_{app} compared to CL-5FAM. P_{app} of the peptide-cargo conjugates was significantly decreased when the spacing between arginines was changed. Sample size n represents the number of transwell replicates: CL-5FAM (n = 7), 5FAM (n = 7), $LRLRLR_8$ (n = 3), all other treatments (n = 4). Data represent mean ± SD. *p < .05, ***p < .001 (One-way ANOVA with post-hoc Tukey HSD test). B. Measured permeability versus theoretical alpha helix hydrophobicity of CL-6TAMRA variants with single leucine substitutions to either tryptophan (W), tyrosine (Y), or valine (V). The position of the leucine substitution (shown in red in the helical wheel diagram) was chosen to maximize the theoretical hydrophobic moment. The dashed line represents P_{app} for 5(6)TAMRA. The apical concentrations were 2.5 μM for the peptide-cargo conjugates and 20 μM for 5(6)TAMRA. n = 12 for each condition. Data represent mean ± SD. The partial correlation between the alpha helix hydrophobicity and P_{app} of peptide-cargo conjugates is not statistically significant when controlling for the hydrophobic moment (r = −0.23, p = .12, Pearson's partial correlation on individual measurements). C. The permeability of CL-6TAMRA peptide variants with different number of RLL repeats. The dashed line represents P_{app} for 5(6)TAMRA. The apical concentrations were 2.5 μM for the peptide-cargo conjugates and 20 μM for 5(6)TAMRA. The highest peptide-cargo conjugate permeability is achieved for two RLL repeats (i.e. CL peptide). CL-3 repeats (n = 3), all other treatments (n = 4). Data represent mean ± SD. ***p < .001 (One-way ANOVA with post-hoc Tukey HSD test). (For interpretation of the references to colour in this figure legend, the reader is referred to the web version of this article.)

$RLLRVLR_8$). This replacement resulted in changes in the calculated hydrophobicity and the hydrophobic moment, while keeping the charge, arginine density, and the length of the alpha helix constant. The results showed that there was no statistically significant correlation between the calculated hydrophobicity and P_{app} and the hydrophobic moment and P_{app}, when controlling for the other variable (Fig. 4B, Fig. S12).

3.5. Polyarginine tail length

As discussed above, we established that the RLLRLLR motif plays an important role in the transcellular cargo delivery. Next, we investigated the contribution of the polyarginine tail of the CL peptide to transcellular transport. We hypothesized that there was an optimal number of arginines to achieve high P_{app}. The CL peptide contains 10 arginines, and 3 of them are part of the helix-like motif and 7 are in the polyarginine tail. Therefore, we synthesized a panel of peptide variants with 1 to 15 arginines in the polyarginine tail (Fig. 5A). Interestingly, decreasing the number of arginines significantly decreased P_{app} of peptide-5FAM conjugates to values close to those for free cargo and Arg_9. The peptide $RLLRLLR_2$, which resembles the helix-like motif but has an extra arginine, and Arg_9 had significantly lower P_{app} than the CL peptide, which suggests that there is a synergistic effect when both sequences are present in the peptide. We observed that the CL peptide with 7 arginines in the polyarginine tail had the highest P_{app}. When we increased the number of arginines to 11 and 15 in the polyarginine tail, P_{app} also decreased. Furthermore, with 11 and 15 arginines, we observed a significant decrease in transepithelial electrical resistance (TEER) across the cell monolayer (Fig. 5B). The significant decrease indicates that these variants compromised the barrier integrity. Indeed, treatment with these peptides resulted in the lowest TEER measured for all of the synthesized peptide variants (Fig. S3).

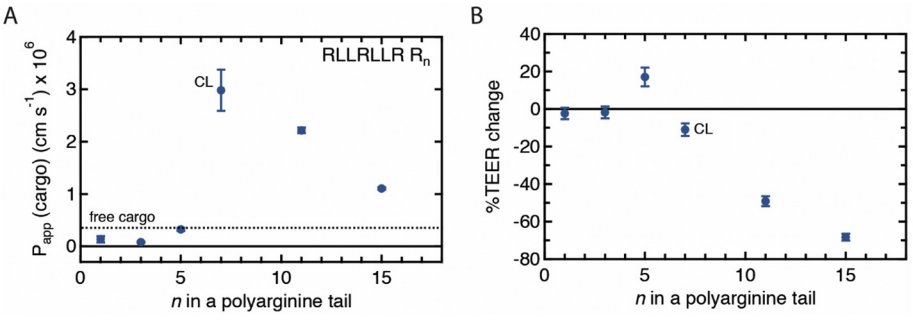

Fig. 5. The effect of the polyarginine tail length on the permeability of peptide-cargo conjugates and change in transepithelial electrical resistance (TEER) across MDCKII cells in a transwell assay. A. The permeability of peptide-cargo conjugates and B. %TEER change after 1-h incubation with CL-5FAM peptide variants with different number of arginines in the polyarginine tail. The dashed line represents P_{app} of 5FAM. The apical concentrations were 2.5 μM for the peptide-cargo conjugates and 10 μM for 5FAM. %TEER change is calculated as (TEER final - TEER initial)/TEER initial x 100%. The MDCKII barrier integrity decreased for N ≥ 11 arginines. The CL peptide has an optimal number of arginines (N = 7) in the polyarginine tail that leads to the maximum P_{app} without compromising the biological barrier integrity. Sample size n represents the number of transwell replicates: CL (n = 6), all other treatments (n = 3). Data represent mean ± SD.

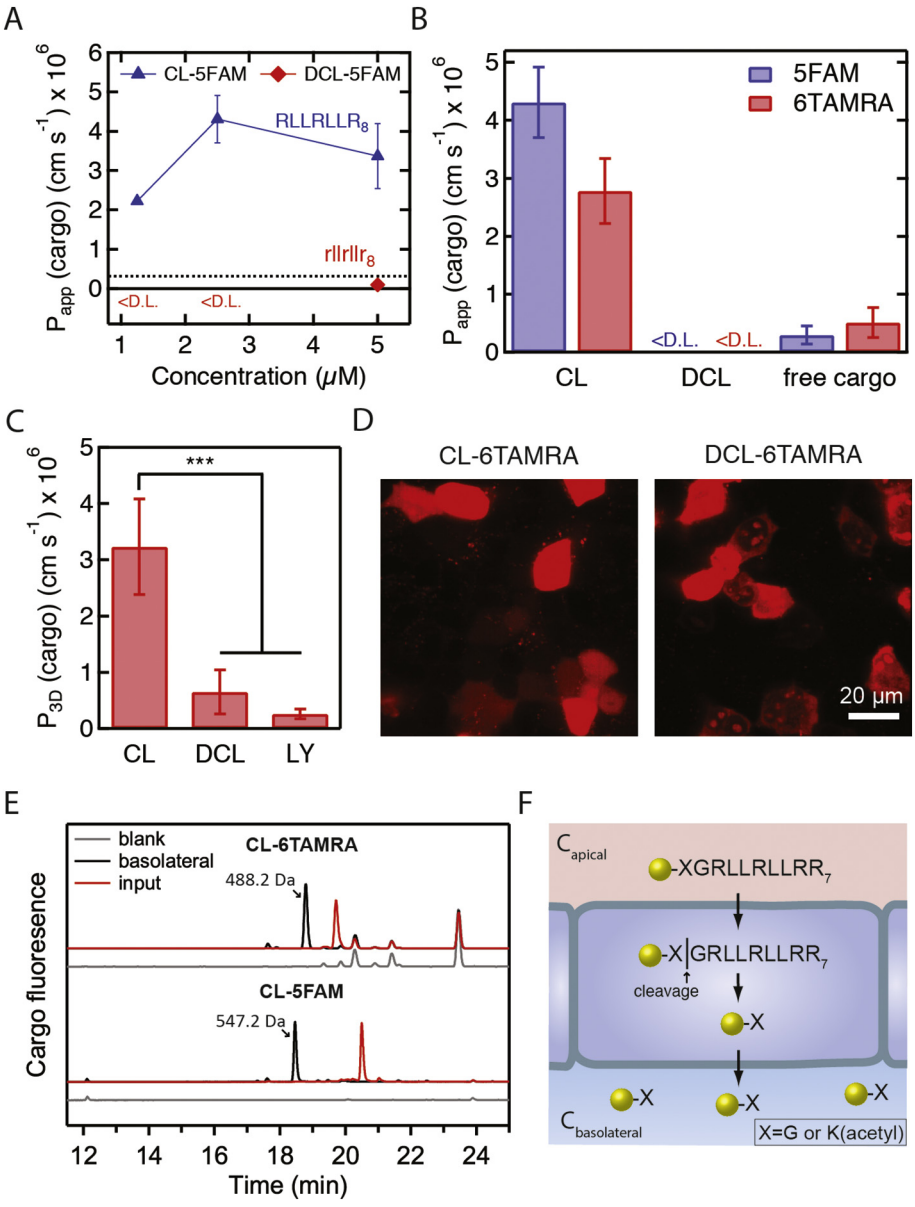

Fig. 6. The role of stereochemistry and proteolysis in transcellular cargo delivery across MDCKII cells. A. The permeability of cargo as a function of concentration for the CL-5FAM peptide and the CL peptide D-isomer (DCL-5FAM). The dashed line represents P_{app} of free 5FAM added at 10 μM apical concentration. < D.L. = below the detection limit. The sample size n represents the number of transwell replicates: 2.5 μM CL-5FAM (n = 6); all other concentrations (n = 3). Data represent mean ± SD. B. The permeability of peptide-cargo conjugates (CL-5FAM, CL-6TAMRA, DCL-5FAM, and DCL-6TAMRA) and for free cargo (5FAM and 5(6)TAMRA). The apical concentrations were 2.5 μM for the peptide-cargo conjugates, 10 μM for 5FAM, and 20 μM for 5(6)TAMRA. The sample size n represents the number of transwell replicates: CL-6TAMRA and DCL-6TAMRA (n = 4), all other treatments (n = 3). Data represent mean ± SD. C. The permeability of peptide-cargo conjugates (CL-6TAMRA and DCL-6TAMRA) and Lucifer yellow in tissue-engineered microvessels. The concentrations were 2.5 μM for the peptide-cargo conjugates and 100 μM for Lucifer yellow. The sample size n represents the number of microvessels: CL-6TAMRA (n = 3), DCL-6TAMRA (n = 3), LY (n = 6). Data represent mean ± SD. D. Confocal microscopy images of the uptake of 2.5 μM CL-6TAMRA and DCL-6TAMRA by MDCKII cells after 1-h incubation at 37 °C (see Fig. S13 for nuclear stain and additional images). Both peptide-cargo conjugates showed diffuse and punctate fluorescence inside the cells. DCL-6TAMRA had an additional localization inside the nucleus, which was not observed for CL-6TAMRA. The D-isomer of the CL peptide can deliver cargo into cells but has low P_{app} across the biological barrier. E. HPLC spectra of the basolateral solution 1 h after introducing CL-5FAM or CL-6TAMRA into the apical chamber. The input solution is the peptide-cargo conjugate solution prior to addition into the apical chamber. The CL-6TAMRA spectrum is expanded 11-fold for comparison to CL-5FAM. F. The proposed mechanism for transcellular transport of CL-cargo conjugates. The CL peptide delivers the conjugated cargo into cells, where the peptide undergoes proteolysis. One of the proteolysis products is the cargo, conjugated to the N-terminal amino acid of the peptide, which exits the cells on the basolateral side, as well as the apical side. (For interpretation of the references to colour in this figure legend, the reader is referred to the web version of this article.)

3.6. Stereochemistry

Arginine-rich peptides are known to have low serum stability, which can limit their applicability for *in vivo* studies and clinical translation [10,41,42]. One strategy to increase peptide serum stability is to introduce D-isomers into the peptide sequence [43]. We therefore synthesized a D-isomer of the CL peptide, designated as the DCL peptide ($rllrllr_8$), to determine whether enhanced transcellular transport is maintained. The DCL peptide exhibited a CD spectrum that was a mirror image of the spectrum of the CL peptide (Fig. S11), indicating that it had the same secondary structure. However, P_{app} for DCL-5FAM was below the detection limit at 1.25 μM and 2.5 μM, and $0.89 \pm 0.07 \times 10^{-7}$ cm s^{-1} at 5 μM, lower than both 5FAM and CL-5FAM (Fig. 6A). P_{app} for both DCL-5FAM and DCL-6TAMRA at a concentration of 2.5 μM were below the detection limit (Fig. 6B). We also measured the permeability for DCL-6TAMRA in the tissue-engineered microvessel. The permeability was $6.5 \pm 3.9 \times 10^{-7}$ cm s^{-1}, not statistically different from Lucifer yellow ($p = .45$, one-way ANOVA with post-hoc Tukey HSD test) (Fig. 6C), and 5-fold lower than for CL-6TAMRA (Fig. 2F). Thus, the use of D-amino acids inhibited the ability of the CL peptide to deliver cargo across an MDCKII monolayer.

Transcellular cargo delivery involves uptake by the cells on the apical side, followed by exit on the basolateral side. We sought to determine whether the cell uptake or the cell exit limits the transcellular cargo delivery for DCL peptide. Some studies have suggested that D-isomers of CPPs have lower cell uptake than L-isomers [44,45]. To assess uptake, we imaged MDCKII cells after incubating with 2.5 μM CL-6TAMRA and DCL-6TAMRA for 1 h. Both CL-6TAMRA and DCL-6TAMRA were taken up by the cells and exhibited punctate and diffuse fluorescence, indicating both passive diffusion and endocytosis (Fig. 6D, Fig. S13). Therefore, DCL-6TAMRA was taken up by the cells but had low P_{app}, suggesting that exit of the cargo out the cell is compromised. Of note, we also observed low P_{app} for the CLr peptide, which has a D-amino acid but also a perturbed secondary structure.

3.7. Proteolysis and the mechanism of transcellular transport

We hypothesized that peptide digestion may be a factor in transcellular transport by the CL peptide. To investigate this possibility, we performed permeability experiments in the transwell assay with CL-6TAMRA and CL-5FAM conjugates and collected the apical and the basolateral solution after the experiment. From HPLC, we observed the presence of one major cargo-containing product in the basolateral chamber and multiple digestion products in the apical chamber (Fig. 6E, Fig. S14). We attempted to block peptide digestion using a proteolysis inhibitor cocktail against serine and cysteine proteases; however, we observed no significant effect on the measured P_{app}, and only a minor decrease in the digestion products in the apical side (Fig. S15). The inhibitor cocktail did not inhibit metalloproteases and aspartic proteases, indicating that they may be involved in peptide proteolysis.

Next, we sought to identify the major cargo-containing digestion product in the basolateral chamber. We purified the basolateral solution from the buffer using HPLC, and then performed LC-MS analysis on the collected fractions (Figs. S16–S17). Elemental composition analysis for CL-5FAM and CL-6TAMRA show that the major product in both cases is the cargo conjugated to the N-terminal amino acid of the linker (Figs. S16–S17): acetylated lysine (CL-5FAM) or glycine (CL-6TAMRA). We also detected a cargo-conjugated fraction with the same retention time in the apical side (Fig. S14B).

Taken together, these results suggest the following cargo delivery mechanism: (i) the CL-cargo conjugate is internalized by epithelial cells in the monolayer; (ii) the conjugate is digested inside the cells generating C-X, where C is cargo and X is the linker amino acid; and (iii) the digestion product, C-X, is transported out of the cells, likely by passive diffusion (Fig. 6F).

4. Discussion

Many CPPs have been developed with the goal of enhancing intracellular delivery. At least 1700 non-redundant CPP sequences have been reported, and more are currently in development [46]. The mechanism of CPP entry has been a topic of intense investigation, but has been difficult to summarize in a few simple rules. CPPs seem to simultaneously utilize different entry mechanisms, such as direct translocation across the plasma membrane and endocytosis. Here we asked if CPPs can be used for delivery of molecular cargo across endothelial layers, where they have to enter cells through the apical membranes and exit through the basolateral membranes. CPPs that have this property can have unique applications in biotechnology, as they could be used to cross the BBB, where tight junctions between the endothelial cells prevent paracellular transport. A few prior studies have either shown low or no enhancement of cargo delivery across the endothelium, or have failed to differentiate transport across the endothelium from sequestration in the endothelium [9]. The mechanisms of transport, and the sequence requirements for transport, have not been the subject of in-depth investigations.

In this study, we discovered that a CPP, denoted the CL peptide, significantly enhanced the delivery of small-molecule cargo across an endothelial cell layer. While there is a size limit to the cargo that it can deliver, it works with both hydrophilic and hydrophobic moieties. Furthermore, we demonstrated that the CL peptide can deliver cargo across a 3D *in vitro* model of an epithelial barrier. Unlike the CL peptide, two well-known CPPs, Arg_9 and TP2, did not enhance cargo delivery. Previous studies in the literature have likewise shown that Tat peptide, one of the first reported CPPs, does not translocate efficiently across Caco-2 cells [47,48].

We further discovered that the cargo-containing molecule that is delivered across the biological barrier is not the original CL-cargo conjugate, but a digestion product. Specifically, the transported entity is the cargo conjugated to the N-terminal amino acid in the linker. Therefore, the epithelial cell machinery cleaves the peptide in the middle of the Gly-Gly or Lys(acetyl)-Gly linker, which connects the peptide and the cargo. Such a proteolysis product has been reported in previous studies of uptake of penetratin and a model amphipathic peptide [47,49].

We found that there are stringent requirements for transcellular translocation. A systematic mutagenesis of the CL peptide, which consists of a helix-like RLLRLLR motif sequence and a polyarginine R_7 tail, showed that the CL peptide has the optimal sequence for transcellular cargo delivery out of all synthesized variants. The mutagenesis of the RLLRLLR motif revealed that: (i) the presence of helix-like secondary structure correlates with high cargo permeability, (ii) arginine spacing by two leucines, as well as two RLL repeats, results in the highest permeability, and (iii) the hydrophobicity and hydrophobic moment of the helix-like motif do not correlate with permeability. Thus, the mutagenesis established the importance of the RLLRLLR motif for permeability. This motif resembles the sequence of the S4 helix (RLVRLLRFLR) of the potassium channel, KvAP [50], which resides in the membrane interface and inserts into the hydrocarbon core upon changes in the electrochemical potential [51]. The S4 helix has been shown to spontaneously translocate across synthetic lipid bilayers [52]. Yet, when we increased the number of RLL repeats in the helix-like motif of CL to closer resemble the S4 helix, we observed a significant decrease in permeability (Fig. 4C).

Further insights into the sequence requirements for translocation were gained by changing the length of the polyarginine tail. Polyarginines are thought to bind to negatively-charged proteoglycans on the cell surface and become internalized either through endocytosis or through direct transport across the cell membrane [7,53]. Previous studies have suggested that cell uptake of polyarginines is maximized for 6–8 residues [54] or 15 residues [55]; however, these studies did not differentiate between internalized and cell surface-bound peptides. We observed that the CL peptide with 7 arginines in the polyarginine tail has the highest permeability, and that the permeability is decreased as the number of arginines in the polyarginine tail was increased to 11 and 15. These experiments showed that the polyarginine tail plays an important role in apical membrane transport and that there is an optimal number of arginines for fast translocation. Based on the previous research with polyarginine peptides we speculate that this number of arginines ensures optimal interaction with the surface proteoglycans [56].

We find that both the helix-like RLLRLLR motif and the polyarginine tail in the CL peptide are required for successful transcellular delivery. We propose that the RLLRLLR motif and the poly-arginine tail each work to enhance translocation and endocytosis, respectively. Indeed, the RLLRLLR motif is also part of the sequence of the peptide TP2, which is known to translocate through lipid bilayers. On the other hand, Arg_9 is known to promote endocytosis. Yet neither TP2 nor Arg_9 potentiated the translocation of cargo in our experiments. Thus, despite being required, neither the RLLRLLR sequence nor the polyarginine tail are sufficient for translocation. There is synergy between the two parts of the CL sequence, which likely reflects synergy between the two entry processes of translocation and endocytosis for the CL peptide.

An important result of this work is that intracellular digestion is necessary for the successful translocation of cargo by the CL peptide. Indeed, the use of D-amino acids inhibited the ability of the CL peptide to deliver cargo across the epithelial monolayer. Yet, DCL-6TAMRA was taken up by the cells, which suggests that the exit of the cargo out of the cells was compromised. These findings demonstrate the importance of a cleavage site within the linker for transcellular cargo delivery. Therefore, the addition of an N-terminal linker, such as the ones used in this work, could improve the transcellular cargo delivery for other existing CPPs. Proteases involved in the cleavage of the dipeptide linker remain to be determined. In our experiments, treatment with a broad spectrum protease inhibitor cocktail did not result in a decrease in permeability, however, it is possible that not all of the components

were sufficiently cell permeable. Since the cleavage occurs after the first N-terminal amino acid, we speculate that aminopeptidases, which cleave at the N-terminal amino acid, may be involved [57]. For example, dipeptide linkers have been previously introduced into prodrugs to be cleaved by cathepsin B, which has aminopeptidase activity [58].

We propose that after intracellular digestion, the cargo and the N-terminal amino acid of the linker leave the cell via passive diffusion through the basolateral and apical membranes. Thus, a requirement for high cargo translocation is the efficient diffusion of the digestion product through the membrane. It is possible, for instance, that the IR800CW cargo was not translocated because it has low permeability across cellular membranes or it interferes with cleavage of the linker. Yet another requirement for translocation is the high accumulation of the digestion product in cells to ensure a high flux through the basolateral membrane. Indeed, in Fig. S18 we see that the intracellular fluorescence, which accounts for both the CL peptide and the digestion product, greatly exceeds the fluorescence outside the cell. We propose that the digestion-induced depletion of peptide inside cells contributes to continuous CL peptide entry into cells and the accumulation of the digestion products.

5. Conclusions

In this study, we discovered that a CPP, denoted the CL peptide, significantly enhanced the delivery of small-molecule cargo across confluent cell monolayers, while other commonly-studied CPPs, including Arg_9 and TP2, did not. The CL peptide has a helix-like motif RLLRLLR and a polyarginine tail R_7, which play a synergistic role in the transcellular cargo delivery. A systematic manipulation of the helix-like motif sequence and the polyarginine tail show that the CL peptide has the optimal sequence of all synthesized variants for transcellular cargo delivery. The results from sequence manipulation suggest that: (i) cell entry of a CPP-cargo conjugate does not necessarily result in fast transcellular cargo delivery, (ii) the presence of helix-like secondary structure correlates with high P_{app}, (iii) an arginine spacing with two leucines results in the highest P_{app}, (iv) the presence of two RLL repeats in the helix-like motif results in the highest P_{app}, (v) the hydrophobicity and hydrophobic moment of the helix-like motif do not correlate with P_{app}, (vi) seven arginines in the polyarginine tail are optimal for high P_{app}, and (vii) the presence of D-amino acids in the peptide correlates with low P_{app}. We also observe that the cargo-containing molecule that is delivered across the confluent cell monolayer is not the original CL-cargo conjugate, but likely a digestion product formed within the cell. The digestion product is the cargo conjugated to the N-terminal amino acid in the linker. This suggests that cells in the biological barrier cleave in the middle of the Gly-Gly or Lys(acetyl)-Gly linker which connects the peptide and the cargo. Thus, our study shows that the digestion of the peptide-cargo conjugate is important for transcellular cargo delivery. We believe that this study can provide new guidelines for the development of novel CPPs for transcellular delivery of cargo.

Funding information

This work was supported by the National Institutes of Health (NINDS 1F31NS101875, NCI 5T32CA153952-08, NIGMS 1R01GM111824, N5106008, NIGM068619, and NINDS R01NS106008), the National Science Foundation (DMR1709892) and the Defense Threat Reduction Agency (HDTRA1-15-1-0046).

Authors' contributions

AK, MB, and RL: Investigation. AK and MB: Data curation and Formal Analysis. AK: Writing - original draft, HC, PS, KH: Writing - review & editing. PS, KH: Conceptualization and Supervision.

Declaration of Competing Interest

The authors declare that they have no competing interests.

Acknowledgements

The content is solely the responsibility of the authors and does not necessarily represent the official views of the funding agencies. The authors thank Dr. Peter Espenshade (Department of Cell Biology, Johns Hopkins School of Medicine) and Dr. Martin Pomper (Department of Radiology, Johns Hopkins Medical Institutions) for the use Odyssey CLx infrared imaging system and Liberty Blue automated microwave peptide synthesizer, respectively. We thank Dr. Sarah Kim and Dr. Gregory Wiedman for assistance with the circular dichroism studies, and Dr. Phil Mortimer for the assistance with LC-MS. We thank Michael Paul for reading the manuscript prior to the publication. We also thank Dr. William Wimley, Dr. Taylor Fuselier, Michael Paul, Dr. Erin Gallagher, and Dr. Luisa Russell for useful discussions.

Appendix A. Supplementary data

Supplementary data to this article can be found online at https://doi.org/10.1016/j.jconrel.2020.05.030.

References

[1] P. Marimuthu, A.G. Schätzlein, Biological barriers: transdermal, oral, mucosal, blood brain barrier, and the blood eye barrier, in: I.F. Uchegbu, A.G. Schätzlein, W.P. Chen, A. Lalatsa (Eds.), Fundamentals of Pharmaceutical Nanoscience, Springer, New York, 2013, p. xiv 598 pages.
[2] W.M. Pardridge, The blood-brain barrier: bottleneck in brain drug development, NeuroRx 2 (2005) 3–14.
[3] T.T. Wager, R.Y. Chandrasekaran, X. Hou, M.D. Troutman, P.R. Verhoest, A. Villalobos, Y. Will, Defining desirable central nervous system drug space through the alignment of molecular properties, in vitro ADME, and safety attributes, ACS Chem. Neurosci. 1 (2010) 420–434.
[4] X. Yi, D.S. Manickam, A. Brynskikh, A.V. Kabanov, Agile delivery of protein therapeutics to CNS, J. Control. Release 190 (2014) 637–663.
[5] D. Ghosh, X. Peng, J. Leal, R. Mohanty, Peptides as drug delivery vehicles across biological barriers, J. Pharm. Investig. 48 (2018) 89–111.
[6] F. Milletti, Cell-penetrating peptides: classes, origin, and current landscape, Drug Discov. Today 17 (2012) 850–860.
[7] W.B. Kauffman, T. Fuselier, J. He, W.C. Wimley, Mechanism matters: a taxonomy of cell penetrating peptides, Trends Biochem. Sci. 40 (2015) 749–764.
[8] L. Vasconcelos, K. Parn, U. Langel, Therapeutic potential of cell-penetrating peptides, Ther. Deliv. 4 (2013) 573–591.
[9] A. Komin, L.M. Russell, K.A. Hristova, P.C. Searson, Peptide-based strategies for enhanced cell uptake, transcellular transport, and circulation: mechanisms and challenges, Adv. Drug Deliv. Rev. 110–111 (2017) 52–64.
[10] S. Stalmans, N. Bracke, E. Wynendaele, B. Gevaert, K. Peremans, C. Burvenich, I. Polis, B. De Spiegeleer, Cell-penetrating peptides selectively cross the blood-brain barrier in vivo, PLoS One 10 (2015) e0139652.
[11] P.M. Fischer, Cellular uptake mechanisms and potential therapeutic utility of peptidic cell delivery vectors: progress 2001-2006, Med. Res. Rev. 27 (2007) 755–795.
[12] E. Gallagher, I. Minn, J.E. Chambers, P.C. Searson, In vitro characterization of pralidoxime transport and acetylcholinesterase reactivation across MDCK cells and stem cell-derived human brain microvascular endothelial cells (BC1-hBMECs), Fluids Barriers CNS 13 (2016) 10.
[13] I. Hubatsch, E.G. Ragnarsson, P. Artursson, Determination of drug permeability and prediction of drug absorption in Caco-2 monolayers, Nat. Protoc. 2 (2007) 2111–2119.
[14] M.I. Bogorad, P.C. Searson, Real-time imaging and quantitative analysis of doxorubicin transport in a perfusable microvessel platform, Integr. Biol. 8 (2016) 976–984.
[15] C. Snider, S. Jayasinghe, K. Hristova, S.H. White, MPEx: a tool for exploring membrane proteins, Protein Sci. 18 (2009) 2624–2628.
[16] J.C. Stewart, Colorimetric determination of phospholipids with ammonium ferrothiocyanate, Anal. Biochem. 104 (1980) 10–14.
[17] R. Lin, P. Zhang, A.G. Cheetham, J. Walston, P. Abadir, H. Cui, Dual peptide conjugation strategy for improved cellular uptake and mitochondria targeting, Bioconjug. Chem. 26 (2015) 71–77.
[18] C.N. Pace, J.M. Scholtz, A helix propensity scale based on experimental studies of peptides and proteins, Biophys. J. 75 (1998) 422–427.
[19] B. Feng, M. West, N.C. Patel, T. Wager, X. Hou, J. Johnson, L. Tremaine, J. Liras, Validation of human MDR1-MDCK and BCRP-MDCK cell lines to improve the prediction of brain penetration, J. Pharm. Sci. 108 (2019) 2476–2483.
[20] S.G. Summerfield, K. Read, D.J. Begley, T. Obradovic, I.J. Hidalgo, S. Coggon,

A.V. Lewis, R.A. Porter, P. Jeffrey, Central nervous system drug disposition: the relationship between in situ brain permeability and brain free fraction, J. Pharmacol. Exp. Ther. 322 (2007) 205–213.
[21] J.D. Irvine, L. Takahashi, K. Lockhart, J. Cheong, J.W. Tolan, H.E. Selick, J.R. Grove, MDCK (Madin-Darby canine kidney) cells: a tool for membrane permeability screening, J. Pharm. Sci. 88 (1999) 28–33.
[22] M.T.Z. Spence, I.D. Johnson, The Molecular Probes Handbook : A Guide to Fluorescent Probes and Labeling Technologies, 11th ed., Live Technologies Corporation, Carlsbad, CA, 2010.
[23] W.C. Wimley, S.H. White, Experimentally determined hydrophobicity scale for proteins at membrane interfaces, Nat. Struct. Biol. 3 (1996) 842–848.
[24] K. Hristova, W.C. Wimley, A look at arginine in membranes, J. Membr. Biol. 239 (2011) 49–56.
[25] K. Melikov, A. Hara, K. Yamoah, E. Zaitseva, E. Zaitsev, L.V. Chernomordik, Efficient entry of cell-penetrating peptide nona-arginine into adherent cells involves a transient increase in intracellular calcium, Biochem. J. 471 (2015) 221–230.
[26] J. He, W.B. Kauffman, T. Fuselier, S.K. Naveen, T.G. Voss, K. Hristova, W.C. Wimley, Direct cytosolic delivery of polar cargo to cells by spontaneous membrane-translocating peptides, J. Biol. Chem. 288 (2013) 29974–29986.
[27] A. Chakrabarti, J.J. Witsenburg, M.D. Sinzinger, M. Richter, R. Wallbrecher, J.C. Cluitmans, W.P. Verdurmen, S. Tanis, M.J. Adjobo-Hermans, J. Rademann, R. Brock, Multivalent presentation of the cell-penetrating peptide nona-arginine on a linear scaffold strongly increases its membrane-perturbing capacity, Biochim. Biophys. Acta 1838 (2014) 3097–3106.
[28] J. Mueller, I. Kretzschmar, R. Volkmer, P. Boisguerin, Comparison of cellular uptake using 22 CPPs in 4 different cell lines, Bioconjug. Chem. 19 (2008) 2363–2374.
[29] J.R. Marks, J. Placone, K. Hristova, W.C. Wimley, Spontaneous membrane-translocating peptides by orthogonal high-throughput screening, J. Am. Chem. Soc. 133 (2011) 8995–9004.
[30] B. Srinivasan, A.R. Kolli, M.B. Esch, H.E. Abaci, M.L. Shuler, J.J. Hickman, TEER measurement techniques for in vitro barrier model systems, J. Lab. Autom. 20 (2015) 107–126.
[31] G. Krishna, K. Chen, C. Lin, A.A. Nomeir, Permeability of lipophilic compounds in drug discovery using in-vitro human absorption model, Caco-2, Int. J. Pharm. 222 (2001) 77–89.
[32] E. De Jong, D.S. Williams, L. Abdelmohsen, J.C.M. Van Hest, I.S. Zuhorn, A filter-free blood-brain barrier model to quantitatively study transendothelial delivery of nanoparticles by fluorescence spectroscopy, J. Control. Release 289 (2018) 14–22.
[34] A.D. Wong, P.C. Searson, Live-cell imaging of invasion and intravasation in an artificial microvessel platform, Cancer Res. 74 (2014) 4937–4945.
[35] Y. Wu, H.W. Huang, G.A. Olah, Method of oriented circular dichroism, Biophys. J. 57 (1990) 797–806.
[36] M. Di Pisa, G. Chassaing, J.M. Swiecicki, Translocation mechanism(s) of cell-penetrating peptides: biophysical studies using artificial membrane bilayers, Biochemistry 54 (2015) 194–207.
[37] P.F. Almeida, A. Pokorny, Mechanisms of antimicrobial, cytolytic, and cell-penetrating peptides: from kinetics to thermodynamics, Biochemistry 48 (2009) 8083–8093.
[38] S.H. White, W.C. Wimley, Hydrophobic interactions of peptides with membrane interfaces, Biochim. Biophys. Acta 1376 (1998) 339–352.
[39] J.S. Appelbaum, J.R. LaRochelle, B.A. Smith, D.M. Balkin, J.M. Holub, A. Schepartz, Arginine topology controls escape of minimally cationic proteins from early endosomes to the cytoplasm, Chem. Biol. 19 (2012) 819–830.
[40] A. Scheller, B. Wiesner, M. Melzig, M. Bienert, J. Oehlke, Evidence for an amphipathicity independent cellular uptake of amphipathic cell-penetrating peptides, Eur. J. Biochem. 267 (2000) 6043–6050.
[41] D. Sarko, B. Beijer, R. Garcia Boy, E.M. Nothelfer, K. Leotta, M. Eisenhut, A. Altmann, U. Haberkorn, W. Mier, The pharmacokinetics of cell-penetrating peptides, Mol. Pharm. 7 (2010) 2224–2231.
[42] J. Grunwald, T. Rejtar, R. Sawant, Z. Wang, V.P. Torchilin, TAT peptide and its conjugates: proteolytic stability, Bioconjug. Chem. 20 (2009) 1531–1537.
[43] J. Fominaya, J. Bravo, A. Rebollo, Strategies to stabilize cell penetrating peptides for in vivo applications, Ther. Deliv. 6 (2015) 1171–1194.
[44] K. Najjar, A. Erazo-Oliveras, D.J. Brock, T.Y. Wang, J.P. Pellois, An L- to D-amino acid conversion in an endosomolytic analog of the cell-penetrating peptide TAT influences proteolytic stability, endocytic uptake, and endosomal escape, J. Biol. Chem. 292 (2017) 847–861.
[45] W.P. Verdurmen, P.H. Bovee-Geurts, P. Wadhwani, A.S. Ulrich, M. Hallbrink, T.H. van Kuppevelt, R. Brock, Preferential uptake of L- versus D-amino acid cell-penetrating peptides in a cell type-dependent manner, Chem. Biol. 18 (2011) 1000–1010.
[46] P. Agrawal, S. Bhalla, S.S. Usmani, S. Singh, K. Chaudhary, G.P. Raghava, A. Gautam, CPPsite 2.0: a repository of experimentally validated cell-penetrating peptides, Nucleic Acids Res. 44 (2016) D1098–D1103.
[47] R. Trehin, H.M. Nielsen, H.G. Jahnke, U. Krauss, A.G. Beck-Sickinger, H.P. Merkle, Metabolic cleavage of cell-penetrating peptides in contact with epithelial models: human calcitonin (hCT)-derived peptides, Tat(47-57) and penetratin(43-58), Biochem. J. 382 (2004) 945–956.
[48] S. Violini, V. Sharma, J.L. Prior, M. Dyszlewski, D. Piwnica-Worms, Evidence for a plasma membrane-mediated permeability barrier to tat basic domain in well-differentiated epithelial cells: lack of correlation with heparan sulfate, Biochemistry 41 (2002) 12652–12661.
[49] C. Palm, M. Jayamanne, M. Kjellander, M. Hallbrink, Peptide degradation is a critical determinant for cell-penetrating peptide uptake, Biochim. Biophys. Acta 1768 (2007) 1769–1776.
[50] Y. Jiang, A. Lee, J. Chen, V. Ruta, M. Cadene, B.T. Chait, R. MacKinnon, X-ray structure of a voltage-dependent K+ channel, Nature 423 (2003) 33–41.
[51] F. Bezanilla, How membrane proteins sense voltage, Nat. Rev. Mol. Cell Biol. 9 (2008) 323–332.
[52] J. He, K. Hristova, W.C. Wimley, A highly charged voltage-sensor helix spontaneously translocates across membranes, Angew. Chem. Int. Ed. Eng. 51 (2012) 7150–7153.
[53] P. Lonn, S.F. Dowdy, Cationic PTD/CPP-mediated macromolecular delivery: charging into the cell, Expert Opin. Drug Deliv. 12 (2015) 1627–1636.
[54] S. Futaki, T. Suzuki, W. Ohashi, T. Yagami, S. Tanaka, K. Ueda, Y. Sugiura, Arginine-rich peptides. An abundant source of membrane-permeable peptides having potential as carriers for intracellular protein delivery, J. Biol. Chem. 276 (2001) 5836–5840.
[55] D.J. Mitchell, D.T. Kim, L. Steinman, C.G. Fathman, J.B. Rothbard, Polyarginine enters cells more efficiently than other polycationic homopolymers, J. Pept. Res. 56 (2000) 318–325.
[56] M. Kosuge, T. Takeuchi, I. Nakase, A.T. Jones, S. Futaki, Cellular internalization and distribution of arginine-rich peptides as a function of extracellular peptide concentration, serum, and plasma membrane associated proteoglycans, Bioconjug. Chem. 19 (2008) 656–664.
[57] A. Taylor, Aminopeptidases: structure and function, FASEB J. 7 (1993) 290–298.
[58] G.M. Dubowchik, R.A. Firestone, Cathepsin B-sensitive dipeptide prodrugs. 1. A model study of structural requirements for efficient release of doxorubicin, Bioorg. Med. Chem. Lett. 8 (1998) 3341–3346.
[60] T Fuselier, W.C. Wimley, Spontaneous Membrane Translocating Peptides: The Role of Leucine-Arginine Consensus Motifs, Biophysical Journal 113 (2017) 835–846, https://doi.org/10.1016/j.bpj.2017.06.070.